npj | flexible electronics

Article

Published in partnership with Nanjing Tech University

https://doi.org/10.1038/s41528-025-00499-0

Strain-invariant frequency-selective metasurface for electromagnetic interference shielding in wearable electronics

Donghee Kim[1,4], Seok Joon Hwang[2,4], Jiwon Ryu[2,3,4], Jun-Chan Choi[1], Woojin Kim[1], Hoon Yeub Jeong[1] ✉, Phillip Lee[2] ✉ & Seungjun Chung[1] ✉

The rapid expansion of wireless communication and data transmission has resulted in highly saturated electromagnetic (EM) environments, where undesired electromagnetic interference (EMI) can compromise signal integrity and lead to malfunctions in electronic systems. However, conventional EMI shielding materials typically attenuate broadband frequencies without selectivity, rendering them incompatible with wireless communication technologies. Moreover, their limited mechanical robustness restricts their applicability in wearable platforms. This study introduces a wearable metasurface-based EMI shielding material that enables selective transmission at 2.4 GHz with simultaneous broadband EMI attenuation across untargeted frequencies. To ensure reliable electromagnetic performance under mechanical deformation, a strain-controlling layer was incorporated to preserve the geometry of the metasurface unit cells. The resulting metasurface maintained consistent frequency-selective transmission at 2.4 GHz and effective EMI shielding under biaxial strain. These findings demonstrate a viable strategy for developing next-generation EMI shielding materials for deformable, wearable, and textile electronic systems through the integration of functional metasurfaces.

As artificial intelligence continues to advance, wearable electronics are being designed to collect and process increasingly large volumes of data[1,2]. This trend has shifted the focus of flexible electronic technologies from solely achieving mechanical robustness to ensuring reliable signal acquisition and processing under extensive mechanical deformation[3–6]. Such developments have enabled a wide range of health-monitoring applications, including the continuous and remote real-time tracking of physiological signals such as heart rate and glucose concentration[7–9]. However, the expansion of wearable and bio-integrated devices has contributed to a highly saturated electromagnetic (EM) environment. Saturated electromagnetic interference (EMI) poses a serious risk to device functionality and user safety by degrading signal fidelity and causing system instability[10,11]. Therefore, there is a critical need for EMI shielding technologies specifically engineered for mechanically dynamic, soft electronic systems. Conventional wearable EMI shielding approaches often employ low-dimensional materials. Two-dimensional (2D) conductive materials such as graphene and MXenes have been extensively investigated due to their high electrical conductivity and large specific surface area, offering substantial EMI shielding effectiveness under static or mildly deformed conditions[12–15]. However, when subjected to continuous mechanical loading such as bending, stretching, or twisting, these materials frequently suffer from mechanical failure, including cracking and delamination, leading to diminished and inconsistent shielding performance over time[16–19]. In addition, their broadband shielding characteristics may unintentionally attenuate signals within frequency ranges essential for wireless communication, thereby restricting their practical utility[20–24]. To address these limitations, there has been increasing interest in selective EMI shielding technologies capable of suppressing unwanted signals while permitting transmission within specific frequency bands vital to the operation of wearable systems. In this context, metasurfaces have emerged as a promising strategy. Composed of periodically arranged

[1]School of Electrical Engineering, Korea University, Seoul, Republic of Korea. [2]Advanced Photovoltaics Research Center, Korea Institute of Science and Technology (KIST), Seoul, Republic of Korea. [3]Department of Materials Science and Engineering, Korea University, Seoul, Republic of Korea. [4]These authors contributed equally: Donghee Kim, Seok Joon Hwang, Jiwon Ryu. ✉e-mail: hoonyeub@korea.ac.kr; phillip@kist.re.kr; seungjun@korea.ac.kr

resonant unit cells, metasurfaces possess engineered electromagnetic responses that enable functionalities such as negative refractive index, cloaking, and arbitrary wave manipulation[25–28]. Among these, frequency-selective metasurfaces are particularly advantageous, as they can be precisely engineered to allow transmission only within designated frequency ranges while suppressing other untargeted frequencies[29–32].

However, maintaining frequency-selective performance under mechanical deformation remains a critical challenge for wearable metasurfaces. Because the electromagnetic response of metasurfaces is highly sensitive to their precise geometric configurations, even minor mechanical perturbations can lead to shifts in the resonant frequency and degradation of filtering performance[33–36]. Furthermore, the conductive networks within the metasurface must remain electrically continuous under repeated and multidirectional strain; any disruption to these pathways can attenuate signal strength and compromise frequency-selective functionality[37,38]. These challenges highlight the requirements for careful material selection and structural design to develop metasurfaces that are mechanically robust and compatible with the functional requirements of next-generation wearable electronic systems.

In this study, a wearable metasurface-based EMI shielding platform was developed to retain frequency-selective transmission capabilities under omnidirectional mechanical deformation, thereby addressing the limitations of conventional approaches. The metasurface design was based on a split-ring resonator (SRR) architecture with geometric parameters optimized to preserve the target resonant frequency independently of the periodicity. This configuration enabled selective transmission of electromagnetic waves at 2.4 GHz, a key frequency for wireless communication, and maintained spectral fidelity even under tensile strain. To achieve mechanical stability and electrical reliability, a silver nanowire (AgNWs) interfacial layer was introduced to enhance adhesion between the intrinsically stretchable eutectic gallium–indium (EGaIn) electrode and the underlying textile substrate. This bonding strategy ensured robust anchoring of the liquid metal, preserved high conductivity, and maintained consistent electrical performance under repeated mechanical loading. Additionally, localized rigidity was incorporated to prevent deformation of the resonant unit cells during strain, without sacrificing overall device stretchability. Using the integration of geometrically engineered metasurfaces and strain-controlled structural features within a mechanically resilient composite architecture, this work demonstrates a wearable EMI shielding material capable of stable frequency-selective transmission under mechanical deformation. These results establish a promising approach for advancing the practical deployment of deformable, frequency-selective metasurfaces in future wearable technologies.

Results

Principle of wearable EMI shielding metasurfaces with frequency selective transmission

Figure 1a presents the structural design of the EMI shielding metasurface, which was fabricated on an elastomeric polydimethylsiloxane (PDMS) substrate and integrated with strain-controlling layers (Polyethylene Terephthalate, PET) to impart localized mechanical rigidity. The metasurface consists of periodically arranged resonators that exhibit distinct electromagnetic behavior. In this work, resonators were patterned on a conductive surface to suppress broadband untargeted electromagnetic waves while selectively transmitting electromagnetic wave at a designated frequency. The metasurface was engineered to allow the transmission of electromagnetic waves at 2.4 GHz, a frequency widely used in wireless communication, while simultaneously providing broadband EMI shielding. The strain-controlling structure plays a critical role in preserving the geometry of the meta-unit cells (Fig. 1b), thereby maintaining frequency selectivity even under biaxial

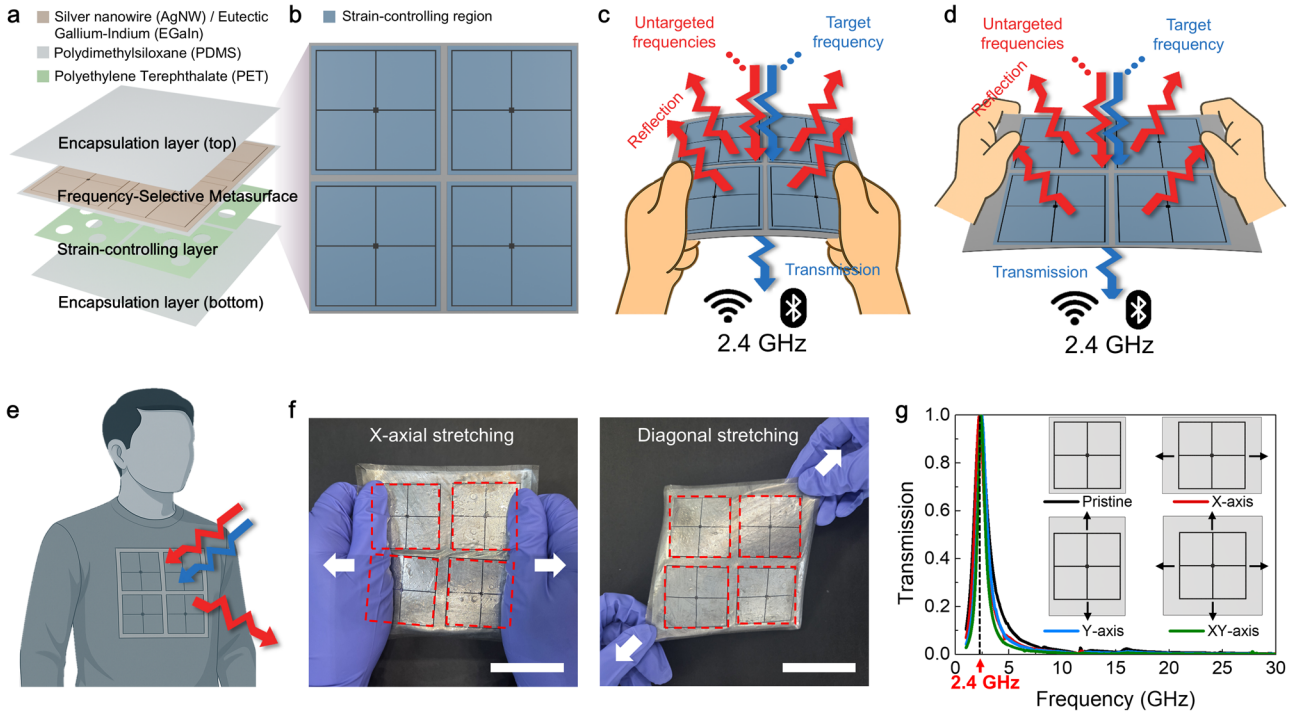

Fig. 1 | Principle of wearable Electromagnetic interference (EMI) shielding metasurfaces with frequency selective transmission. a Expanded view of the multilayer configuration of the EMI-shielding metasurface. (False colors). **b** Schematic of the EMI shielding metasurface composed of silver nanowire (AgNW)/ Eutectic Gallium-Indium (EGaIn) conductive materials patterned on a Polydimethylsiloxane (PDMS) substrate with strain-controlling structures. **c** A schematic of the EMI shielding metasurface illustrating consistent selective transmission of the target frequency (blue) while blocking untargeted frequencies (red) under mechanical bending. **d** A schematic of the EMI shielding metasurface illustrating consistent selective transmission of the target frequency while blocking untargeted frequencies under mechanical stretching. **e** A schematic of a seamlessly integrated wearable EMI shielding metasurface into clothing. **f** Images of fabricated EMI shielding metamaterial under uniaxial stretching (left: X-axial direction, right: diagonal direction) Scale bars: 5 cm. **g** Simulated transmission spectra of our EMI shielding metasurface at 30% mechanical strain, showcasing consistent electromagnetic performance even under mechanical strain.

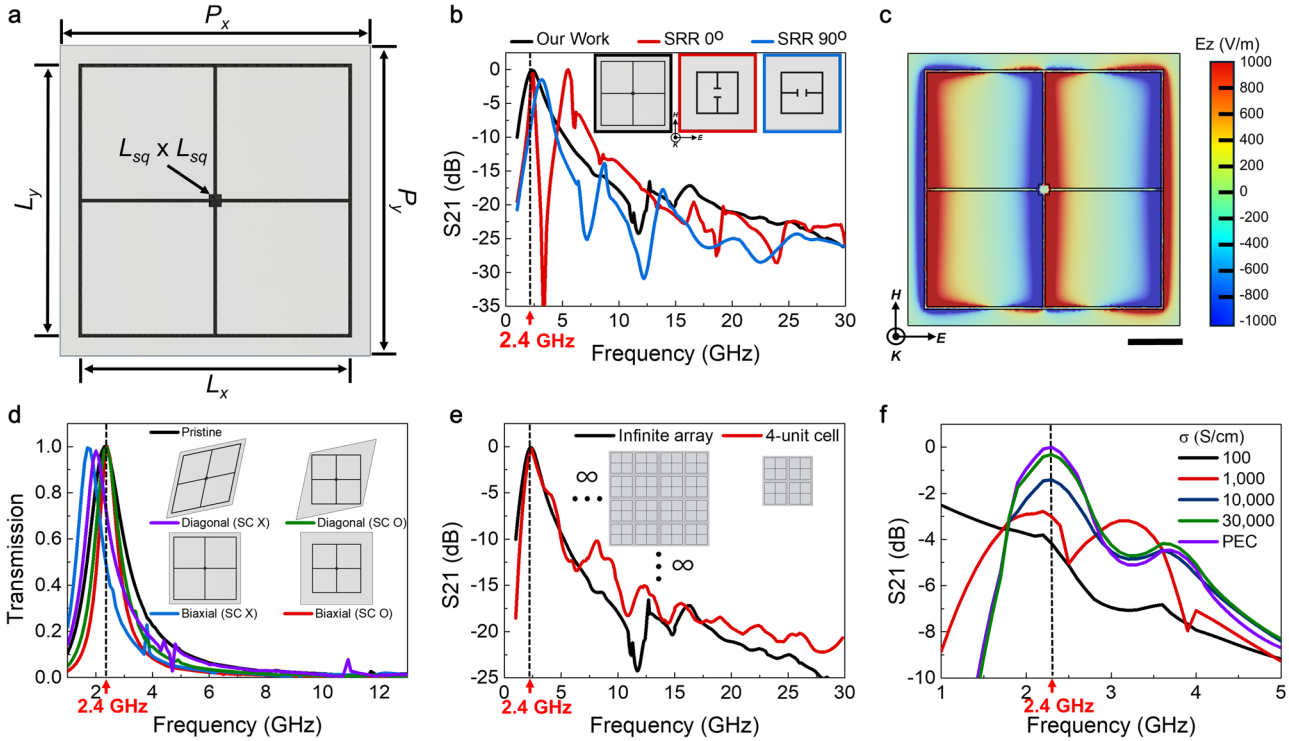

Fig. 2 | Design of metasurfaces for wearable EMI shielding with 2.4 GHz wave transmission. a Design and geometric parameters of the optimized meta-unit cell. **b** Simulated transmission spectra comparing Split Ring Resonator (SRR)-based metasurfaces under different polarization angles and the optimized design under plane wave incidence with x-polarized electric field. The (SRR)-based metasurface has a polarization-dependent electromagnetic response owing to the asymmetry, whereas our optimized metasurface induce only a 2.4 GHz dipole resonance transmission peak without polarization dependency. **c** Z-component of the electric field profile of the optimized metasurface at 2.4 GHz resonance, demonstrating the dipole resonance field profile; scale bar: 1 cm. **d** Simulated transmission spectra of optimized metasurface comparing cases with and without strain-controlled structures at 30% mechanical strain. Without strain control, diagonal (purple) and biaxial (blue) strains cause significant resonance shifts. In contrast, strain-controlled structures preserve resonance near 2.4 GHz under both diagonal (green) and biaxial (red) strains, consistent with the pristine case (black). **e** Simulated transmission spectra comparing an infinite array (black) with a finite 4-unit cell array (red), demonstrating comparable performance. **f** Simulated transmission spectra of the optimized 4-unit cell metasurface at varying electrical conductivities.

mechanical deformation such as bending and stretching, as illustrated in Fig. 1c, d. This large-area, soft metasurface can be seamlessly integrated into wearable platforms, ensuring stable electromagnetic performance (Fig. 1e). Figure 1f demonstrates the structural integrity of the meta-unit cells under mechanical strain along both the x-axis and diagonal directions, made possible by the strain-controlling framework. Furthermore, simulated transmission spectra (Fig. 1g) confirm that selective transmission at 2.4 GHz is maintained under both 30% uniaxial and biaxial strain, thereby validating the capability to retain signal fidelity in deformable wearable electronic platforms.

Design of metasurfaces for EMI shielding with 2.4 GHz wave transmission

Figure 2a depicts the optimized meta-unit cell design for EMI shielding with frequency-selective transmission, along with its geometric parameters: periodicities (P_x, P_y), lengths (L_x, L_y), line width (L_w) and center square length (L_{sq}). These parameters were determined using electromagnetic finite element method (FEM) simulations to achieve resonance at 2.4 GHz, yielding the following dimensions: $P_x = 50$ mm, $P_y = 50$ mm, $L_x = 44$ mm, $L_y = 44$ mm, $L_w = 0.5$ mm and $L_{sq} = 2$ mm on a 450 μm-thick dielectric layer consisted of 110 μm-thick PET and then encapsulating with PDMS. The meta-unit cell design is based on an SRR, a commonly used structure in metasurface engineering due to its strong subwavelength resonance characteristics[39] (Supplementary Fig. 1). To effectively suppress broadband electromagnetic interference while allowing signal transmission at the target frequency, the metasurface must exhibit strong dipole resonance at the target frequency and suppress higher-order resonances such as quadrupole and hexapole modes. Otherwise, additional resonances may lead to the unintended transmission at untargeted frequencies. In addition, to ensure stable operation under varying environmental conditions, the metasurface must maintain consistent electromagnetic behavior regardless of the polarization state of the incident wave. The meta-unit cell geometry was therefore carefully optimized to meet these functional requirements, by varying the geometrical parameters (L_{sq} and L_w) as shown in Supplementary Fig. 2. Figure 2b presents the simulated transmission spectra for both the conventional SRR-based and the optimized metasurface designs. The SRR-based metasurface exhibited a sharper resonance peak (higher quality factor) with smaller unit cell; however, it also generated an undesired quadrupole resonance at a higher frequency, thereby impairing frequency selectivity (red line). Although rotating the SRR structure by 90° eliminated the quadrupole mode, it shifted the resonance away from 2.4 GHz, reducing transmission amplitude and potentially compromising wireless communication reliability (blue line). In contrast, the optimized metasurface demonstrated robust frequency-selective transmission centered at 2.4 GHz over a broad frequency range (1–30 GHz), and under both polarization configurations (black line), confirming its effectiveness. Figure 2c shows the Z-component of the electric field at 2.4 GHz, clearly illustrating the dipole resonance mode. Supplementary Fig. 3 further supports these findings by comparing electric field distributions and transmission spectra between the optimized and SRR-based metasurfaces.

To effectively implement a metasurface as an EMI shielding material for wearable platforms, it is essential to maintain signal integrity under mechanical deformation. However, ensuring consistent electromagnetic performance in deformable conditions remains a significant challenge, as the electromagnetic response of metasurfaces is highly sensitive to the geometry of individual meta-unit cells. Figure 2d presents the simulated

transmission spectra of the optimized metasurface under 30% mechanical strain, comparing configurations with and without strain-controlling structures. In the absence of such structures, mechanical deformation alters the shape of the meta-unit cells, resulting in elongation along the strain direction and contraction in the transverse direction due to Poisson's effect[40,41]. This geometric distortion leads to a pronounced shift in the resonant frequency. For instance, under diagonal strain, the resonant frequency shifted from the target value of 2.4 GHz to 2.0 GHz (purple line), while biaxial strain, which causes uniform expansion of the entire structure, shifted the resonance further to 1.7 GHz (blue line). Such deviations can impair signal transmission and lead to communication failure. In contrast, the integration of strain-controlling structures allows the applied strain to be absorbed by the peripheral regions surrounding the meta-unit cells, preserving their original geometry while altering only the periodicity. The resulting transmission spectra (green and red lines) under both diagonal and biaxial strain demonstrate minimal change in resonant frequency, confirming that signal integrity and frequency selectivity are effectively maintained. This validation supports that the strain-controlling design allows the stable electromagnetic performance under mechanical deformation. This strain-invariance can be further analyzed through the unit cell and its coupling characterization. Resonant frequency of unit cells can be characterized with overall inductance (L) and capacitance (C) as below.

$$f_{unit\ cell} = \frac{1}{2\pi\sqrt{LC}} \tag{1}$$

In the case of periodic array, additional coupling terms (L_c, C_c) were added due to the coupling from the adjacent resonators. Resonant frequency of periodic array becomes as below.

$$f_{array} = \frac{1}{2\pi\sqrt{(L+L_c)(C+C_c)}} \tag{2}$$

Due to the broad dipole resonance, coupling effects have little influence on the resonant frequency as the periodicity varies from 50 mm to 65 mm, maintaining over 90% transmission amplitude at 2.4 GHz (Supplementary Fig. 4a, b). In other words, the resonant frequency of our optimized metasurface is dominated by the intrinsic resonant frequency of its unit cell. Without strain-controlling structures, applied strain induces distortion of the unit cell, resulting in deviation of geometry-dependent resonant frequency of the unit cell (Supplementary Fig. 4c), and consequently altering resonant frequency of metasurfaces (Fig. 2d). Moreover, conventional electromagnetic analyses of metasurfaces assume an infinite periodic array. However, implementing a large number of unit cells in practice can be impractical for wearable platforms due to spatial and integration constraints. Figure 2e compares the simulated transmission spectra of the optimized metasurface configured as an infinite array and as a 2 × 2 array (4-unit cells). The results confirm that even with only 4-unit cells, the dipole resonance can still be effectively excited, demonstrating strong signal transmission at 2.4 GHz while concurrently suppressing unwanted frequencies. This enables the metasurface to be miniaturized to compact dimensions (e.g., 10 cm × 10 cm), is particularly advantageous for integration into wearable platforms. Even with only a 4-unit cell, the transmission spectra of the finite array closely resemble those of the infinite periodic array (Supplementary Fig. 5a), supporting the reasonable approximation of the finite structure as an infinite array. Simulated spectra of 4-unit cell array exhibited strain-invariant frequency-selectivity under 30% uniaxial and biaxial strain, similar to the infinite array case from Supplementary Fig. 5b, c. In addition to geometric considerations, the electrical conductivity of the conductive material is a critical factor in achieving effective electromagnetic performance. Insufficient conductivity can significantly impair resonance characteristics. Figure 2f presents the simulated transmission spectra of the optimized 4-unit cell metasurface for various conductivity values. The simulations indicate that a conductivity of ~30,000 S/cm is required to achieve a dipole resonance comparable to that of an idealized perfect electric conductor (PEC) as shown in Supplementary Fig. 6. Additionally, this level of conductivity must be maintained under mechanical deformation to ensure stable electromagnetic functionality in flexible and stretchable applications. Note that detailed simulation information is described in Method section.

Characterization of the AgNWs-assisted EGaIn and fabrication of wearable EMI shielding metasurface

EGaIn is a promising material for wearable EMI shielding metasurfaces due to its ability to retain high electrical conductivity under mechanical strain. However, its poor adhesion to elastomeric substrates, e.g. PDMS, can lead to delamination and loss of electrical continuity, compromising performance. To address this limitation, a AgNW interfacial layer was introduced to improve bonding between EGaIn and PDMS. Figure 3a compares the electrical conductivities of pristine EGaIn (red) and AgNW-assisted EGaIn (blue). The conductivity of the AgNW-assisted EGaIn reached 31,000 S/cm which is comparable to that of pristine EGaIn and above the threshold required to support strong dipole resonance in the optimized metasurface (Supplementary Fig. 7). Furthermore, measurements of normalized resistance (R/R_0) under mechanical strain demonstrate that the inclusion of the AgNW bonding layer is essential for preserving electrical integrity, as it effectively prevents delamination and disruption of the EGaIn layer during deformation. When subjected to tensile strain up to 90% corresponding to the fracture strain of the PDMS substrate, the normalized resistance of the AgNW-assisted EGaIn electrode remained substantially more stable than that of pristine EGaIn, indicating the preservation of the conductive network (Fig. 3b). Furthermore, under cyclic tensile deformation at 30% strain, the AgNW-assisted EGaIn exhibited negligible changes in normalized resistance, in contrast to the pristine EGaIn, which showed a 4.8-fold increase in resistance after 2000 cycles (Fig. 3c). The inset images in Fig. 3c reveal the surface morphology following cyclic loading, clearly demonstrating the improved adhesion and structural integrity of the AgNW-assisted composite. For the successful realization of wearable EMI shielding metasurfaces, both the selection of mechanically and electrically stable conductive materials and the adoption of precise fabrication techniques are essential. Figure 3d illustrates the multilayer architecture of the fabricated metasurface. The metasurface is embedded between a top PDMS encapsulation layer and a bottom PDMS layer, with a patterned polyethylene terephthalate (PET) strain-controlling layer incorporated to preserve the geometry of the meta-unit cells during mechanical deformation. The PET layer was structured using a 355 nm ultraviolet (UV) laser to create through-hole patterns, which improved adhesion between the PET and PDMS encapsulation layers. The EMI shielding metasurface layer was formed using the AgNW-assisted EGaIn electrode, sandwiched between the structural layers. To achieve high-resolution patterning of the metasurface, a laser lift-off technique was employed, wherein a 355 nm UV laser was used to locally ablate the PDMS layer beneath the electrode, enabling simultaneous detachment of the overlying conductive material (Fig. 3e). Scanning electron microscopy (SEM) and energy-dispersive X-ray spectroscopy (EDS) elemental mapping confirmed that the patterned resonator structures accurately matched the simulated optimal linewidth (~500 μm). Additionally, the elemental distributions of silicon (Si, green), gallium (Ga, cyan), and indium (In, red) verified that the conductive material was effectively removed from the patterned regions (Fig. 3f). The consistent pattering resolution *via* laser processing was inspected through statistical analysis, revealing line width with an average of 484.65 μm and standard deviation of 9.9 μm. Simulated transmission spectra of optimized metasurface confirmed consistent electromagnetic behavior with feasible line widths during laser patterning process (Supplementary Fig. 8). Further fabrication details are provided in the Methods section and in Supplementary Figs. 9–11. Figure 3g presents a bottom-view image of the fabricated 2 × 2 metasurface, presenting distinctly visible metasurface pattern and the

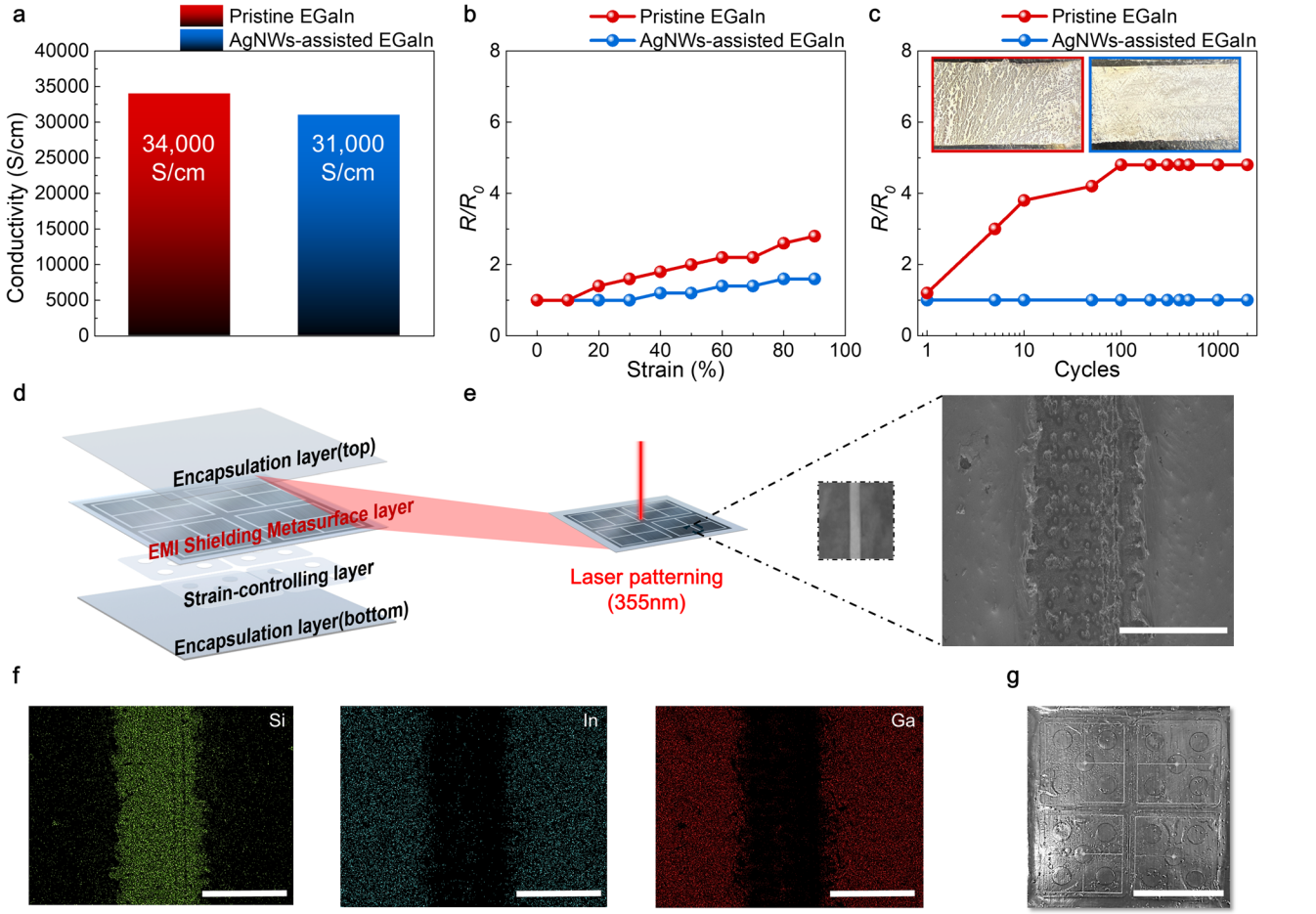

Fig. 3 | Characterization of AgNW-assisted EGaIn and fabrication of the wearable EMI shielding metasurface. a Electrical conductivity comparison between AgNW-assisted EGaIn and pristine EGaIn electrodes. **b** Normalized resistance change (R/R_0) under uniaxial tensile strain, comparing AgNW-assisted EGaIn electrode and pristine EGaIn electrode. **c** Comparison of resistance variation during 30% cyclic tensile deformation (2000 cycles) between the AgNW-assisted EGaIn electrode and the pristine EGaIn electrode. **d** Schematic of the multilayer structure of the EMI shielding metasurface device. **e** Schematic of the laser patterning process, along with SEM image and EDS elemental mapping of the patterned region; scale bar: 500 μm. **f** EDS images showing the precise patterning of the conductive layers and distribution of Si (green), In (cyan), and Ga (red) atoms; scale bars: 500 μm. **g** Bottom-view image of the fabricated 2 × 2 metasurface; scale bar: 5 cm.

four integrated strain-controlling structures (4.8 cm × 4.8 cm). The dielectric layer was fabricated to a sufficiently thin thickness (450 μm) to minimize signal attenuation from dielectric loss. In addition, it offers both mechanical comfort and facile strain control, arising from the large mismatch in elastic moduli between PET (3 GPa) and PDMS (1.23 MPa). The simulated strain distribution of our 2 × 2 metasurface under 0–30% applied strain validates the local rigidity of the strain-controlling region, while effectively redistributing the strain toward the peripheral regions (Supplementary Fig. 12).

Electromagnetic performance of wearable EMI shielding metasurface with selective electromagnetic wave transmission

Figure 4a compares the simulated (dashed line) and experimentally measured (solid line) transmission spectra of the 4-unit cell metasurface (black) and unpatterned sheet (red), showing good agreement in selectively transmitting the target frequency while effectively attenuating unwanted frequency ranges. To simulate a realistic application scenario, the metasurface was positioned directly in front of Antenna 2, mimicking its attachment to clothing for the purpose of shielding incident electromagnetic waves (Fig. 4b). Three different samples were measured to ensure reproducibility of our EMI shielding metasurface, exhibiting consistent frequency-selective transmission with broadband EMI shielding performance (Supplementary Fig. 13). Our wearable metasurface demonstrated not only exhibit frequency-selective transmission but also comparable broadband shielding effectiveness considering its thickness (overall 450 μm with 10 μm of pattern), compared with other soft EMI shielding materials (Supplementary Table S1). Supplementary Fig. 14 further depicts the seamless integration of the EMI shielding metasurface into wearable garments. Figure 4c demonstrates the conformal attachment of the metasurface on textile, maintaining the integrity of the meta-unit cell geometry even during bending, without observable distortion. Ensuring reliable performance across different temperatures is essential for wearable applications in diverse climatic environments[42–44]. Owing to the negligible change in the conductivity of the AgNW-assisted EGaIn electrode, the metasurface exhibited consistent electromagnetic performance over a wide temperature range (Supplementary Fig. 15 and Fig. 2f). In addition to standardized transmission measurements (Fig. 4b), the EMI shielding performance of our metasurface was further evaluated under practical, real-world conditions. Specifically, Wi-Fi signal amplitudes at 2.4 GHz and 5 GHz from the router were measured using embedded software on a smartphone (Fig. 4d). These measurements were conducted in both unstretched (pristine) and mechanically stretched states, with the receiving antenna in the used smartphone shielded from the Wi-Fi router using either a conventional EMI shielding material (a 1-mm-thick aluminum plate) or the metasurface (Supplementary Fig. 16 and Supplementary Videos 1 and 2). As shown in Fig. 4e, f, conventional shielding materials significantly attenuated both the 2.4 GHz and 5 GHz signals. In contrast, the metasurface allowed the 2.4 GHz Wi-Fi signal to pass through with minimal attenuation, maintaining a signal amplitude

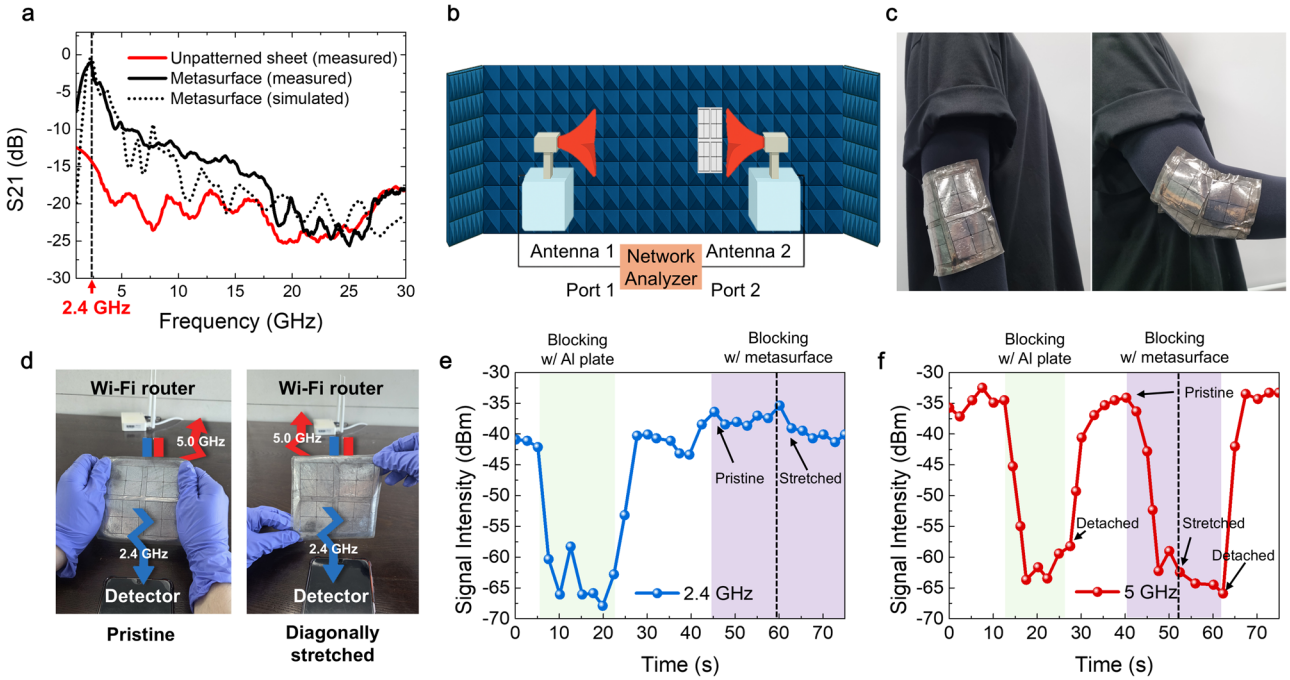

Fig. 4 | Electromagnetic performance of the real-world wearable EMI shielding metasurface with frequency-selective transmission. a Comparison between simulated (dotted) and measured (solid) transmission spectra of optimized EMI shielding metasurface (black) and unpatterned sheet (red). Fabricated metasurface exhibits selective 2.4 GHz electromagnetic wave transmission with simultaneous shielding of untargeted electromagnetic waves. **b** Schematic of the standardized measurement setup for the measured data in (**a**). **c** Images of wearable metasurface integrated into clothing, showing distortion-free meta-unit cell structures under a bending motion. **d** Images of measurement setup utilizing commercial Wi-Fi routers and smartphones under realistic conditions. The metasurface was placed in front of the smartphone to block the Wi-Fi signal from the router in the pristine (left) and diagonally stretched (right) states. **e** Measured signal intensity of 2.4 GHz Wi-Fi signal blocked by either the conventional shielding material (1-mm-thick Al plate, green-shaded) or metasurface (purple-shaded). The white-shaded regions indicate unblocked states. **f** Measured signal intensity of the 5 GHz Wi-Fi signal blocked by either the Al plate (green-shaded) or metasurface (purple-shaded). The white-shaded regions indicate unblocked states. Additional measurements were performed using the metasurface in a diagonally stretched state, as indicated in (**e** and **f**).

comparable to that observed in the unshielded condition. Importantly, this selective transmission was preserved even when the metasurface was subjected to mechanical stretching. Meanwhile, the 5 GHz signal was effectively blocked under both pristine and strained conditions, demonstrating its frequency-selective shielding capability. These findings validate the practical applicability of the proposed EMI shielding metasurface, confirming its suitability for integration into wearable electronic platforms while ensuring robust wireless communication at designated frequencies.

Discussion

In this study, a wearable metasurface based on SRR architecture was developed to achieve frequency-selective EMI shielding on a textile-compatible platform. The metasurface was engineered to exhibit a strong resonance at 2.4 GHz while effectively suppressing higher-order resonances and minimizing polarization dependence, thereby enabling broadband EMI shielding with selective electromagnetic wave transmission. To ensure stable performance under mechanical deformation, strain-controlling structures were incorporated into the metasurface design. These structures preserved the geometric integrity of the meta-unit cells during stretching and bending, allowing the electromagnetic response to remain consistent in dynamic conditions. Notably, simulations demonstrated that a compact array consisting of only 4-unit cells exhibited transmission characteristics comparable to those of an infinite array, confirming the practical feasibility of implementing the metasurface in space-constrained, wearable applications. AgNW-assisted EGaIn was employed as the conductive material to achieve both high electrical conductivity and mechanical compliance. The AgNW interfacial layer significantly enhanced the adhesion between EGaIn and the PDMS substrate, maintaining electrical conduction under strain. Precise laser patterning was utilized to define the resonator geometries, and the conductive layer was integrated into a multilayer structure with embedded strain-control features to prevent meta-unit cell distortion. The fabricated metasurface was evaluated both in a controlled measurement setup using horn antennas and in a realistic scenario involving a smartphone and Wi-Fi router. The results confirmed reliable and selective transmission of 2.4 GHz signals while suppressing untargeted frequencies, even under applied mechanical strain. Strain-invariance through strain-controlling strategy highlights its general applicability to other metasurface designs and across diverse frequency regimes, including the mmWave and even the terahertz range (Supplementary Figs. 17, 18). Overall, this study demonstrates the practical integration of frequency-selective metasurfaces into wearable platforms and introduces a scalable design approach for next-generation EMI shielding materials that combine mechanical flexibility with electromagnetic functionality.

Methods

Materials

Glass substrates (1 mm thick, 120 × 120 mm) and PET films were obtained from Daihan Scientific Group. EGaIn alloy was purchased from Sigma-Aldrich, and PDMS (Sylgard™ 184) was sourced from Dow Corning. Hexane, isopropanol alcohol (IPA) and deionized (DI) water were acquired from Daejung Chemicals. Clevios™ PH 1000 was obtained from Heraeus. A AgNW solution (A70, research grade 0.5, in 100 mL ethanol, 5 mg/mL) was purchased from Novarials. Nonwoven wipers (WW-2109) were supplied by Kmbiz.

Electromagnetic simulation

Electromagnetic simulations were performed using the RF Module of COMSOL Multiphysics. Periodic boundary conditions and port settings were applied to model the metasurface. The conductive elements were initially modeled as perfect electric conductors. The metasurface was made

up bottom 40-μm-thick PDMS, 110-μm-thick PET strain-controlling layer, metasurface layer, and 300-μm-thick PDMS encapsulating layer. Dielectric constants of materials were set as 2.7 with loss tangent of 0.02 in both PDMS and PET. To simulate deformation, periodicity was increased along the strain axis in the case of metasurfaces with strain-controlling structures. For configurations without strain control, both the periodicity and the geometry of the meta-unit cells were modified: elongation occurred along the direction of applied strain, while contraction occurred along the transverse direction, consistent with the Poisson's ratio of PDMS. For simulations involving the 4-unit cell metasurface, a perfectly matched layer (PML) condition was used in place of periodic boundary conditions. The receiving port was apart 20 mm from the metasurface to simulate practical situation, where metasurface is attached to clothing. To investigate the influence of finite conductivity, a 10-μm-thick transition boundary layer with a specified conductivity value was applied to model the conductive material.

Mechanical simulation

Mechanical simulation was performed with structural mechanics module in COMSOL Multiphysics. The 2 × 2 metasurface structure was modeled same with the electromagnetic simulation. Elastic modulus was set as 3 GPa for PET strain-controlling layer, and 1.23 MPa for PDMS. Poisson's ratio was set as 0.37 for PET, and 0.5 for PDMS. A fixed boundary condition was applied to left end surface of the structure, while a prescribed displacement was applied at the right end surface, deforming the structure under strain range of 0–30%.

Electrical and electromechanical characterization

Electrical conductivity (S/cm) was measured at room temperature using a 4-point probe system (Loresta-GX MCP-T700, NITTOSEIKO ANALYTECH). The electrode thickness was ~10 μm, as determined by cross-sectional SEM (Supplementary Fig. 7). Tensile strain-dependent resistance (R/R_0) measurements were conducted using rectangular samples with dimensions of 1 cm × 2.5 cm. Each sample was clamped at both ends (0.25 cm from each edge) using a dial-type tensile tester. Electrical contact was established by attaching copper tape to the grips, which were connected to a multimeter for real-time resistance measurements under varying strain conditions.

Fabrication of wearable EMI shielding metasurfaces

A clean glass substrate was first coated with a PH1000 solution (IPA:PH1000 = 2:1 v/v) via spin-coating at 400 rpm for 10 s, followed by drying at 100 °C for 5 min to form a sacrificial layer. A layer of PDMS prepolymer was then spin-coated at 1000 rpm for 30 s and cured at 100 °C for 20 min. To enhance surface adhesion for subsequent processing steps, the cured PDMS was treated using an ultraviolet ozone (UVO) cleaner (Ahtech LTS) for 2000 s, generating surface hydrophilic Si–OH functional groups. Following surface activation, an AgNW dispersion was spray-coated using a 3 mm nozzle and annealed at 60 °C for 10 min. EGaIn was subsequently drop-cast onto the surface and uniformly spread using a nonwoven wiper; excess material was removed by spin-coating at 1000 rpm for 30 s. The metasurface pattern was defined using UV laser ablation (ML-UVL, Gain Laser, 355 nm, 5 W), which selectively removed the underlying PDMS while simultaneously lifting off the conductive electrode, thereby forming the meta-unit cell structures. A second PDMS layer was then spin-coated and cured at 100 °C. The entire laminate stack was immersed in DI water for 5 min and gently delaminated from the glass substrate (Supplementary Fig. 9).

For multilayer integration, a fresh glass substrate was prepared following the same cleaning and sacrificial coating procedure. A PDMS/hexane mixture (1:1 v/v) was spin-coated at 1000 rpm for 30 s and partially cured at 100 °C for 1 min to form the top encapsulation layer (Supplementary Fig. 10). The previously fabricated EMI metasurface layer was then inverted and laminated onto the partially cured PDMS layer, followed by complete curing at 100 °C. Another PDMS/hexane layer was spin-coated and partially cured under the same conditions. A PET film (48 × 48 mm), pre-patterned with laser-cut through-holes for strain-controlling structures, was laminated onto the partially cured PDMS and fully cured. Finally, a bottom PDMS encapsulation layer was applied by spin-coating and fully cured. The entire device was immersed in DI water for 5 min and delaminated from the glass substrate to yield the completed EMI shielding metasurface (Supplementary Fig. 11).

Microwave measurement

Microwave measurements were performed using two horn antennas: a 3117 double-ridged waveguide antenna (ETS-Lindgren, 1–18 GHz) and an SAR-1834031432-KF-S2-DR antenna (ERAVANT, 18–30 GHz), both connected to a vector network analyzer (N5227B, Keysight Technologies). The antennas were positioned 1.6 m apart, with an absorbing wall placed behind them to minimize signal reflections. For simulation of a wearable application scenario, the metasurface sample was mounted on a polystyrene panel and placed directly in front of one of the receiving horn antennas. To absorb bypassing electromagnetic waves, 30 × 30 cm pyramidal microwave absorber was placed around the sample. For the measurements shown in in Fig. 4d–f, a commercial Wi-Fi router and a smartphone (SM-G996, Samsung Electronics) were used. The smartphone was positioned 1.5 m away from the Wi-Fi router. During testing, either a 1 mm-thick aluminum plate or the fabricated EMI shielding metasurface was placed directly in front of the smartphone's receiving antenna to block incoming Wi-Fi signals. Measurements were conducted under both pristine and diagonally stretched conditions to assess the metasurface's performance under mechanical deformation. The received signal strength at 2.4 GHz and 5 GHz was recorded using embedded signal-monitoring software on the smartphone (Supplementary Fig. 16 and Supplementary Videos 1–2).

Data availability

The data supporting the plots in this study and other findings of this study are available from the corresponding authors upon reasonable request.

Received: 22 July 2025; Accepted: 2 November 2025;
Published online: 17 December 2025

References

1. Ates, H. C. et al. End-to-end design of wearable sensors. *Nat. Rev. Mater.* **7**, 887–907 (2022).
2. Linh, V. T. N. et al. Advances in wearable electronics for monitoring human organs: Bridging external and internal health assessments. *Biomaterials* **314**, 122865 (2024).
3. Nan, Z. et al. Flexible electromagnetic interference shields: materials, structure and multifunctionalization. *Mater. Sci. Eng. R. Rep.* **160**, 100823 (2024).
4. Zong, J. Y. et al. A wearable multifunctional fabric with excellent electromagnetic interference shielding and passive radiation heating performance. *Compos. Pt. B Eng.* **225**, 109299 (2021).
5. Zou, K. et al. Efficient electromagnetic interference shielding of flexible Ag microfiber sponge/polydimethylsiloxane composite constructed by blow spinning. *Compos. Sci. Technol.* **220**, 109281 (2022).
6. Shi, Y. et al. Advanced functional electromagnetic shielding materials: a review based on micro-nano structure interface control of biomass cell walls. *Nano Micro Lett.* **17**, 3 (2025).
7. Chang, T. et al. Highly integrated watch for noninvasive continual glucose monitoring. *Microsyst. Nanoeng.* **8**, 25 (2022).
8. Vaghasiya, J. V., Mayorga-Martinez, C. C. & Pumera, M. Wearable sensors for telehealth based on emerging materials and nanoarchitectonics. *npj Flex. Electron.* **7**, 26 (2023).
9. Mansour, M., Darweesh, M. S. & Soltan, A. Wearable devices for glucose monitoring: A review of state-of-the-art technologies and emerging trends. *Alex. Eng. J.* **89**, 224–243 (2024).
10. Li, L. et al. Wearable EMI shielding composite films with integrated optimization of electrical safety, biosafety and thermal safety. *Adv. Sci.* **11**, 2400887 (2024).

11. Pan, D. et al. Biomimetic wearable sensors: emerging combination of intelligence and electronics. *Adv. Sci.* **11**, 2303264 (2024).
12. Iqbal, A., Sambyal, P. & Koo, C. M. 2D MXenes for Electromagnetic Shielding: A Review. *Adv. Funct. Mater.* **30**, 2000883 (2020).
13. Orts Mercadillo, V. et al. Electrically conductive 2D material coatings for flexible and stretchable electronics: a comparative review of graphenes and MXenes. *Adv. Funct. Mater.* **32**, 2204772 (2022).
14. Han, M. et al. Beyond $Ti_3C_2T_x$: MXenes for electromagnetic interference shielding. *ACS Nano.* **14**, 5008–5016 (2020).
15. Cai, Z. et al. Multifunctional Mxene/holey graphene films for electromagnetic interference shielding, Joule heating, and photothermal conversion. *Compos. Pt. B-Eng.* **251**, 110477 (2023).
16. Yang, Y. et al. $Ti_3C_2T_x$ MXene-graphene composite films for wearable strain sensors featured with high sensitivity and large range of linear response. *Nano Energy* **66**, 104134 (2019).
17. Zeng, Z. H. et al. Porous and Ultra-Flexible Crosslinked MXene/Polyimide Composites for Multifunctional Electromagnetic Interference Shielding. *Nano Micro Lett.* **14**, 59 (2022).
18. Yu, Y. et al. Environmentally Tough and Stretchable MXene Organohydrogel with Exceptionally Enhanced Electromagnetic Interference Shielding Performances. *Nano Micro Lett.* **14**, 77 (2022).
19. Duan, Y. et al. Enhanced EMI Shielding and Mechanical Stability via Deformable MXene-rNGO Conductive Networks in Superelastic PDMS composite. *Compos. Pt. B Eng.* **295**, 112198 (2025).
20. Cheng, J. et al. Recent Advances in Design Strategies and Multifunctionality of Flexible Electromagnetic Interference Shielding Materials. *Nano Micro Lett.* **14**, 80 (2022).
21. Kuila, C., Maji, A., Murmu, N. C., Kuila, T. & Srivastava, S. K. Recent advancements in carbonaceous nanomaterials for multifunctional broadband electromagnetic interference shielding and wearable devices. *Carbon* **210**, 118075 (2023).
22. Li, Y. et al. Meter-Scale Wearable Multifunctional Core-Shell Nanofiber Textiles for Ultra-Broadband Electromagnetic Interference Shielding and Infrared Stealth. *Adv. Mater.* **37**, 2501485 (2025).
23. Liu, J., Yu, M. Y., Yu, Z. Z. & Nicolosi, V. Design and advanced manufacturing of electromagnetic interference shielding materials. *Mater. Today* **66**, 245–272 (2023).
24. Jung, J. et al. Highly stretchable and transparent electromagnetic interference shielding film based on silver nanowire percolation network for wearable electronics applications. *ACS Appl. Mater. Interfaces* **9**, 44609–44616 (2017).
25. Tian, J. & Cao, W. Reconfigurable flexible metasurfaces: from fundamentals towards biomedical applications. *PhotoniX* **5**, 2 (2024).
26. An, S. et al. Energy-efficient dynamic 3D metasurfaces via spatiotemporal jamming interleaved assemblies for tactile interfaces. *Nat. Commun.* **15**, 7340 (2024).
27. Qiu, T. et al. Vision-driven metasurfaces for perception enhancement. *Nat. Commun.* **15**, 1631 (2024).
28. Liu, X. et al. Electrically programmable pixelated coherent mid-infrared thermal emission. *Nat. Commun.* **16**, 1665 (2025).
29. Prasad, N. et al. Flexible Metamaterial-Based Frequency Selective Surface with Square and Circular Split Ring Resonators Combinations for X-Band Applications. *Mathematics* **11**, 800 (2023).
30. Nguyen, D. T., Lee, J.-N., Moon, J. I. & Jung, C. W. Single-Layer Frequency-Selective Surface on Window Glass for 5G Indoor Communications. *IEEE Antennas Wirel. Propag. Lett.* **23**, 1558–1562 (2024).
31. Jeong, H. Y. et al. Tunable Resonance and Phase Vortices in Kirigami Fano-Resonant Metamaterials. *Adv. Mater. Technol.* **5**, 2000234 (2020).
32. Chen, J., Zhang, H., Ji, H., Wang, F. & Xiao, H. Origami tunable frequency selective fabric and its tuning mechanism. *Compos. Pt. A Appl. Sci. Manuf.* **164**, 107257 (2023).
33. Li, F. et al. Flexible intelligent microwave metasurface with shape-guided adaptive programming. *Nat. Commun.* **16**, 3161 (2025).
34. Zhuang, X. et al. Active terahertz beam steering based on mechanical deformation of liquid crystal elastomer metasurface. *Light Sci. Appl.* **12**, 14 (2023).
35. Reeves, J. B. et al. Tunable infrared metasurface on a soft polymer scaffold. *Nano Lett.* **18**, 2802–2806 (2018).
36. Han, Z. et al. MEMS-actuated metasurface Alvarez lens. *Microsyst. Nanoeng.* **6**, 79 (2020).
37. Feng, Y. et al. Fabrication and modulation of flexible electromagnetic metamaterials. *Microsyst. Nanoeng.* **11**, 14 (2025).
38. Jeong, H. Y. et al. Directly Printed 3D Soft Microwave Plasmonic Enhanced-Q Resonators by Decoupling from Lossy Media. *Adv. Mater.* **37**, 2418182 (2025).
39. Degl'Innocenti, R. et al. Low-bias terahertz amplitude modulator based on split-ring resonators and graphene. *ACS Nano.* **8**, 2548–2554 (2014).
40. Choi, J.-C. et al. Bidirectional Zero Poisson's Ratio Elastomers with Self-Deformable Soft Mechanical Metamaterials for Stretchable Displays. *Adv. Funct. Mater.* **34**, 2406725 (2024).
41. Choi, J.-C. et al. Depth-Modulus Engineered Meta-Elastomers for Multiaxial Strain Programming in Stretchable Displays. *Small Struct.* **6**, 2400513 (2025).
42. Li, W. et al. Large-scale ultra-robust MoS2 patterns directly synthesized on polymer substrate for flexible sensing electronics. *Adv. Mater.* **35**, 2207447 (2023).
43. Li, W. et al. Microsecond-scale transient thermal sensing enabled by flexible Mo1 − xWxS2 alloys. *Research* **7**, 0452 (2024).
44. Malakooti, M. H. et al. Liquid metal supercooling for low-temperature thermoelectric wearables. *Adv. Funct. Mater.* **29**, 1906098 (2019).

Acknowledgements

This work was supported by the National Research Foundation of Korea (NRF) grant funded by the Korea government (MSIT) (Nos. RS-2023-NR076982, RS-2024-00416978, RS-2024-00459468).

Author contributions

D.K., S.J.H., H.Y.J., P.L. and S.C. conceived the study. D.K. and H.Y.J. optimized the metasurface and conducted an electromagnetic FEM simulation. J.R. conducted the material characterization and fabricated a wearable EMI shielding metasurface. D.K., J.R., J.-C.C. and W.K. curated the data. S.J.H., H.Y.J., P.L. and S.C. wrote the manuscript. H.Y.J., P.L. and S.C. supervised this study. All authors discussed the results and approved the manuscript.

Competing interests

The authors declare no competing interests.

Additional information

Supplementary information The online version contains supplementary material available at https://doi.org/10.1038/s41528-025-00499-0.

Correspondence and requests for materials should be addressed to Hoon Yeub Jeong, Phillip Lee or Seungjun Chung.